Perpendicular ferromagnetic resonance in soft cylindrical elements: Vortex and saturated states

V. Castel
Université de Bretagne Occidentale, Laboratoire de Magnétisme de Bretagne CNRS, 29285 Brest, France and University of Groningen, Physics of Nanodevices, Zernike Institute for Advanced Materials, Nijenborgh 4, 9747 AG, Groningen, The Netherlands

J. Ben Youssef
Université de Bretagne Occidentale, Laboratoire de Magnétisme de Bretagne CNRS, 29285 Brest, France

F. Boust
Onera - The French Aerospace Lab, F91123 Palaiseau, France

R. Weil
Université Paris Sud, Laboratoire de Physique des Solides, UMR 8502, bat 510, 91405 Orsay, France

B. Pigeau, G. de Loubens, V. V. Naletov, and O. Klein
Service de Physique de l'État Condensé (CNRS URA 2464), CEA Saclay, 91191 Gif-sur-Yvette, France

N. Vukadinovic*
Dassault Aviation, 78 quai Marcel Dassault, 92552 St-Cloud, France
(Received 21 February 2012; published 22 May 2012)

Linear magnetic excitations in perpendicularly magnetized micrometer-sized disks have been investigated in detail both in the saturated and the vortex states using ferromagnetic resonance spectroscopy and micromagnetic simulations. Broadband ferromagnetic resonance spectra measured in disk arrays reveal a set of discrete resonance lines associated with the dipole-exchange spin-wave modes quantized by the disk edge in the saturated state and several new resonance lines (up to four) with negative slopes for the frequency-field dispersion relation $\omega(H_z)$ in the vortex state at intermediate magnetic fields. The micromagnetic simulations performed for a Py disk array (regime of negligible coupling between the disks) allow us to identify the four excitations occurring in the deformed vortex state as vortex core, disk edge, and coupled vortex core/disk edge modes, and to reproduce very satisfactorily their experimental $\omega(H_z)$ curves. In addition, the nonlinear frequency dependence of the resonance linewidth for the predominant coupled vortex core/edge mode experimentally observed is in agreement with the numerical prediction. These findings are finally confirmed by magnetic resonance force microscopy measurements conducted on an isolated NiMnSb disk. The remarkable similarity between the experimental results coming from two magnetic systems and using two different microwave probes demonstrates the robustness of the physical phenomenon.

DOI: 10.1103/PhysRevB.85.184419 PACS number(s): 75.40.Gb, 75.40.Mg

I. INTRODUCTION

The high-frequency linear excitations in confined magnetic structures exhibiting nonuniform magnetization distributions are subject to a growing interest in the field of nanomagnetism. Among the multiple magnetic structures, the disk elements supporting a vortex state are the most studied. This micromagnetic state can be viewed as an in-plane curling magnetization with a central region, the vortex core, where the magnetization points out of plane. It corresponds to the ground state for submicrometer- and micrometer-sized soft ferromagnetic disks with a thickness L_z and a disk radius R satisfying $L_z > \Lambda$ and $R \gg \Lambda$, where $\Lambda = \sqrt{A/(2\pi M_s^2)}$ is the exchange length, A the exchange constant, and M_s the saturation magnetization.[1] The vortex state is characterized by two topological quantities: the vortex core polarization (direction of the vortex core magnetization) and the vortex chirality (rotational direction of the in-plane magnetization).

Extensive investigations of the radio-frequency (RF) field-driven magnetic excitations in vortex-state circular elements have been conducted during the last decade. It is now well-established both theoretically and experimentally that the zero-field linear excitation spectrum consists of a low-frequency (sub-GHz range) vortex translation mode corresponding to the gyrotropic motion of the vortex core as a whole around the disk center[2–6] and a set of radial and azimuthal modes spreading mainly outside the vortex core and occurring beyond a few GHz.[7–14] These spin-wave (SW) modes are quantized due to the finite lateral size of the disk and are labeled using the (l,n) mode indices[15] referring to the number of nodes of the out-of-plane magnetization component along the azimuthal and radial directions inside the disk, respectively. In addition, a coupling between the vortex translation mode and the azimuthal modes has been evidenced leading to a frequency splitting of the azimuthal modes.[16–19] Moreover, the high-frequency responses of magnetostatically coupled micro/nanodisks (small interdisk distance) with a vortex state were also analyzed.[20–25] Depending on the vortex polarizations and chiralities, coupled vortex translation modes were theoretically[20,22] and numerically[25] pointed out giving rise to collective spin-wave modes with a band structure for an infinite array of disk elements.[21,23]

On the other hand, the excitation spectrum of a vortex-state disk in the presence of a polarizing magnetic field has been less addressed. One can distinguish the case of an in-plane field (in the sample's plane) that breaks the rotational symmetry and that of a perpendicular field (perpendicular to the sample's plane) that preserves the rotational symmetry. In the former case, the in-plane magnetic field induces a shift of the vortex core and new localized modes associated with the deformed vortex state were revealed.[12,13,26,27] In the latter case, the linear field evolution of the resonance frequency for the vortex translation mode was numerically predicted[28] and experimentally observed.[29] But, to our knowledge, no investigations were reported regarding the excitation spectrum in wide perpendicular magnetic field and frequency ranges.

This paper aims at investigating the linear magnetic excitations existing in perpendicularly magnetized micrometer-sized ferromagnetic disks by means of ferromagnetic resonance (FMR) spectroscopy and micromagnetic simulations. Detailed comparisons between experimental and numerical spectra are reported. Much attention is paid to the resonance lines occurring at intermediate perpendicular magnetic fields and exhibiting negative slopes for the dispersion curves $\omega(H_z)$, where ω is the angular frequency and H_z is the amplitude of the polarizing magnetic field.

This paper is organized as follows. Section II gathers the experimental details in terms of sample preparation and characterizations for arrays of Permalloy (Py) disks. Representative perpendicular FMR spectra recorded for such disk arrays are then displayed. Section III is devoted to the micromagnetic simulations. The main features of the used micromagnetic codes are first recalled. Then, results of computed magnetization curves and susceptibility spectra are presented. Section IV addresses the comparisons between the experimental and numerical FMR spectra for Py disk arrays over broad magnetic field and frequency ranges. In particular, the frequency dependencies of the resonance fields and linewidths are analyzed in detail. These main findings are confirmed by magnetic resonance force microscopy (MRFM) measurements carried out on a single NiMnSb micrometer-sized disk. These additional results are reported in Sec. VI. Conclusions are drawn in Sec. VII.

II. EXPERIMENT

A. Sample preparation and magnetic characterizations

Square arrays of Permalloy ($Ni_{80}Fe_{20}$) disks with thickness $L_z = 50$ nm, various diameters $2R = 1,2$, and 5 μm, and edge-to-edge spacing $x = 2\,\mu$m were fabricated using electron beam lithography (EBL) and etching techniques from a RF sputtered $Ni_{80}Fe_{20}$(50 nm)/Au(2 nm) film on a 2-inch Si wafer. Scanning electron microscopy (SEM) and atomic force microscopy (AFM) were carried out to characterize the disk arrays (diameter, interdisk spacing). As an example, the SEM image of the array with $2R = 1$ μm is shown in the inset in Fig. 1. Introducing the reduced interdisk distance $\delta = x/(2R)$, the smallest disk corresponds to $\delta = 2$ (regime of negligible dipolar coupling between the disks) and the largest one to $\delta = 0.4$ (regime of significative dipolar coupling).[30] The total patterned area was 3×3 mm^2, a size required to obtain a sufficiently large magnetic volume for broadband FMR measurements.

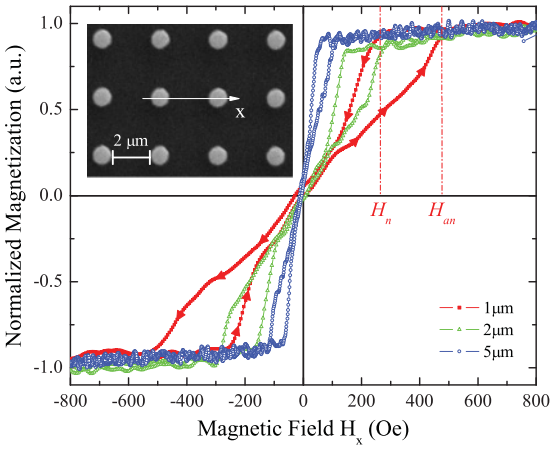

FIG. 1. (Color online) Experimental in-plane magnetization curves for arrays of Py disks with various diameters $2R = 1,2$, and 5 μm from MOKE measurements. The interdisk distance is fixed at $x = 2\,\mu$m and the disk thickness is $L_z = 50$ nm. The inset corresponds to a SEM image of the array with $2R = 1$ μm. The arrows indicate the sense of the magnetic field variation.

First, the main magnetic parameters of the Py film were experimentally determined. The saturation induction $4\pi M_S$ was extracted from the vibrating sample magnetometer (VSM) at room temperature and was found to be equal to 9720 G. The in-plane uniaxial anisotropy field constant H_K was extracted from the zero-field permeability spectrum along the in-plane hard axis measured by means of a single-coil permeameter[31,32] resulting in $H_K = 4$ Oe.

Broadband FMR measurements were performed in perpendicular configuration (static magnetic field H_z applied along the film normal) within the frequency range 1–25 GHz using a highly sensitive wideband resonance spectrometer with a nonresonant 50 Ω microstrip reflection line. This one supplies a RF exciting magnetic field with a linear polarization. To enhance the sensitivity of the FMR signal, a field modulation (amplitude much smaller than the FMR linewidth) and a lock-in technique were employed yielding the power absorption derivative spectrum dP_a/dH.

For the perpendicular configuration, the resonance condition for the uniform precession mode in an extended film leads to the linear variation of the angular frequency ω as a function of the polarizing magnetic field H_z: $\omega = \gamma(H_z - 4\pi M_S + H_K)$. The peak-to-peak resonance linewidth ΔH_{pp} is related to the angular frequency by the linear relation: $\Delta H_{pp} = \Delta H_{pp,0} + 2\alpha\omega/(\gamma\sqrt{3})$, where γ is the gyromagnetic ratio, $\Delta H_{pp,0}$ is the zero-frequency residual contribution to the linewidth of extrinsic origin, and α is the Gilbert damping parameter. These expressions were used to fit the experimental linear variations of $\omega(H_z)$ and $\Delta H_{pp}(\omega)$ and the following parameters were deduced: $\gamma = (1.861 \pm 0.002) \times 10^7$ rad Oe^{-1} s^{-1}, $\Delta H_{pp,0} = 2.4 \pm 0.9$ Oe, and $\alpha = (7.1 \pm 0.1) \times 10^{-3}$.

Next, magneto-optical Kerr effect (MOKE) measurements were carried out for the disk arrays. Figure 1 displays the in-plane magnetization curves recorded for the three disk

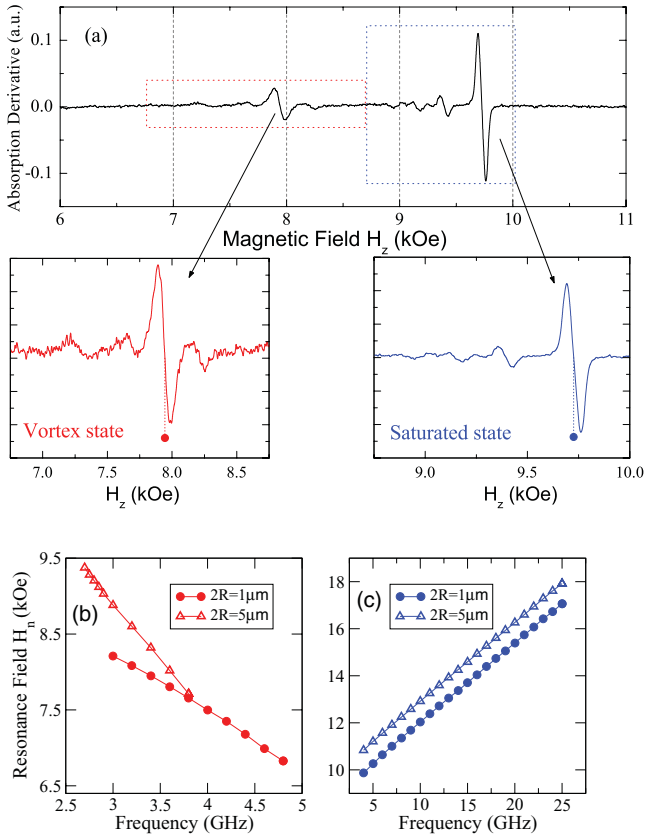

FIG. 2. (Color online) (a) Experimental microwave absorption spectra (derivative form) for the array with $2R = 1$ μm recorded at $f = 3.5$ GHz using a broadband FMR spectrometer. The insets are magnifications of the spectrum in the field range associated with the vortex and the saturated states. (b) Frequency dependencies of resonance fields for the main peak in the vortex state. (c) Frequency dependencies of the fundamental peak in the saturated state. For each case, two disk diameters are considered $2R = 1$ μm and 5 μm.

diameters. These hysteresis loops exhibit the signature of vortex state with a vanishing remanence at zero field, a linear variation $M(H_x)$ at low fields (reversible displacement of the vortex), and abrupt changes associated with the magnetization reversal through the nucleation (nucleation field H_n) and annihilation (annihilation field H_{an}) of the vortex.[1,30] In addition, increasing the disk diameter (reducing δ) leads to a decrease of both $|H_n|$ and $|H_{an}|$, a reduced field distance $|H_n - H_{an}|$, and an increase of the initial susceptibility (slope of the linear variation at low fields) in agreement with the previously reported results.[30]

B. Perpendicular FMR spectra in disk arrays

FMR measurements were then conducted for the disk arrays. Figure 2(a) shows a typical power absorption derivative spectrum dP_a/dH recorded at $f = 3.5$ GHz for the array of disks with $2R = 1$ μm. Multiple resonance lines are observed both for the unsaturated and saturated regimes [see the enlargements of the spectrum in Fig. 2(a)]. For the unsaturated regime, one main resonance line is detected accompanied by two subsidiary lines on the low-field side and another one on the high-field side. One striking feature is the decrease of the resonance field as the frequency increases as displayed in Fig. 2(b) for the main resonance line. In addition, the slope of the variation depends on the disk size. The resonance field decreases more rapidly for the largest disk diameter. On the other hand, the FMR spectrum for the saturated regime reveals one main resonance line and several peaks with decreasing amplitudes on the low-field side. In this case, the resonance field increases linearly with frequency and the slope remains unchanged whatever the disk diameter [see Fig. 2(c)]. Only a field shift occurred when the disk diameter varies. A detailed analysis of theses results by means of micromagnetic simulations and quantitative comparisons with experimental data form the core of the next two sections.

III. MICROMAGNETIC MODELING

A. Model

The high-frequency response of magnetic nanoelements is investigated by means of micromagnetic simulations using two 3D homemade codes described elsewhere.[33] The first code computes an equilibrium magnetization configuration by integrating the Landau-Lifshitz (LL) equation in the time domain using a second-order Taylor scheme and an optimized time step. The second one solves the LL equation linearized around the equilibrium magnetization configuration (small-amplitude motion regime) in the frequency domain. It computes the local dynamic susceptibility tensor $\chi_{ij}(\mathbf{r},\omega)$, $i,j = x,y,z$, which depends on both space and angular frequency, and then the dynamic susceptibility tensor averaged over the element's volume V, $\chi_{ij}(\omega) = \langle \chi_{ij}(\mathbf{r},\omega) \rangle_V$, $i,j = x,y,z$, which connects the high-frequency response of a magnetic configuration $\delta\mathbf{m}$ to a weak exciting RF magnetic field $\delta\mathbf{h}$ such as $\delta\mathbf{m} = \overline{\chi}\,\delta\mathbf{h}$. These codes were previously used to investigate the microwave dynamics of vortex-state[28] and bubble-state[34] elements. In what follows, $\delta\mathbf{h}$ will be assumed uniform and applied either along the symmetry axis of the disk element (z axis) or in the disk plane. Due to the rotational symmetry of the element, the in-plane susceptibility spectra will be expressed using the circular polarization basis resulting in the $\chi_\pm$ element defined as $\chi_\pm = 1/2[(\chi_{xx} + \chi_{yy}) \pm i(\chi_{yx} - \chi_{xy})]$. Hereafter, only the imaginary part of $\chi_\pm$ will be displayed. The FMR spectra are then determined using the general expression of the microwave power absorbed by the sample of volume V from the RF magnetic field:[35,36] $P_a = \langle \int_V dV \delta\mathbf{h} \cdot \frac{d\delta\mathbf{m}}{dt} \rangle_{\text{time average}}$, which takes the equivalent form $P_a = 1/2\,\Re[i\omega \int_V dV \delta\tilde{\mathbf{h}} \cdot \delta\tilde{\mathbf{m}}^*]$ using the complex notation with a harmonic time dependence $\delta\mathbf{h} = \delta\tilde{\mathbf{h}} e^{i\omega t}$ and $\delta\mathbf{m} = \delta\tilde{\mathbf{m}} e^{i\omega t}$, where $\delta\tilde{\mathbf{h}}$ and $\delta\tilde{\mathbf{m}}$ are complex vectors and the asterisk denotes the complex conjugation.

It should be remarked that for a uniform excitation in a perpendicularly magnetized disk, the SW mode will be labeled using only the radial index n. The azimuthal index will be implicitly assumed to be always equal to $l = 0$. Lastly, the magnetic samples are discretized using a regular cubic mesh. The mesh sizes $\Delta_i, i = x,y,z$ are equal to 7.8 nm which is close to the exchange length $\Lambda = 5.7$ nm by adopting the value of the exchange constant $A = 1.3 \times 10^{-6}$ erg/cm. This mesh size is a good compromise between the accuracy and the time consumed computing the magnetic excitation spectra in the saturated regime and in the unsaturated regime at intermediate

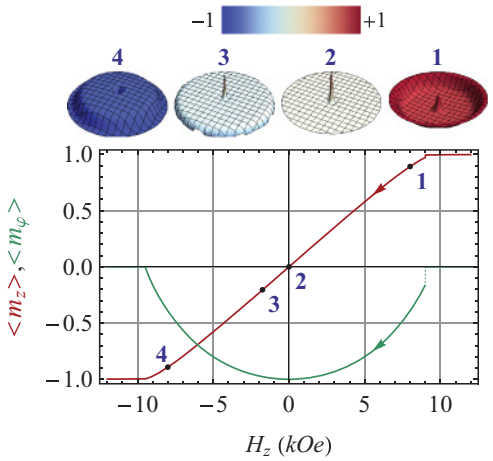

FIG. 3. (Color online) Computed perpendicular magnetization curves (half cycle) for the space-averaged normalized components $\langle m_z\rangle$ and $\langle m_\phi\rangle$. The 3D images correspond to the static magnetization configurations for four decreasing values of the magnetic field. The disk array with $2R = 1$ μm is considered.

values of the magnetic field applied along the z axis.[37] The sizes of the simulated disk are hence $2R = 998.4$ nm and $L_z = 46.8$ nm.

B. Results

This part intends to provide a broad picture of the static and dynamic properties of a single Py disk ($2R = 1$ μm) under a perpendicular static magnetic field. The comparisons with the experimental data will be addressed in Sec. IV.

1. Magnetization curves

The computed perpendicular magnetization curves (half cycles) for the space-averaged normalized components $\langle m_z\rangle$ and $\langle m_\phi\rangle$, where $m_i = M_i/M_s$, $i = z,\phi$, and M_ϕ is the orthoradial magnetization component in the disk plane, are displayed in Fig. 3. In addition, the equilibrium magnetizations for four decreasing magnetic field values are also visualized (top images in Fig. 3). It should be noted that these equilibrium magnetization configurations do not vary significantly along the z coordinate for this low aspect ratio disk ($\beta = L_z/R = 0.1$). For large magnetic field values, $H_z > H_s \simeq 9$ kOe, where H_s is the perpendicular saturation field, the disk is uniformly magnetized along the $+z$ axis ($\langle m_z\rangle = 1$). When the magnetic field is reduced below H_s, a nonuniform magnetization state emerges (point 1 in Fig. 3) with larger values of m_z within disk center region (premise of the vortex core) and at the disk edge. The magnetization configuration can be considered as a deformed vortex state. By further decreasing the magnetic field, the vortex core develops and m_z diminishes outside the vortex core. At zero field, a classical vortex state is stabilized with a vortex core region with $m_z > 0$, a dip area around the vortex core with $m_z < 0$, and a peripheral zone where $m_z = 0$ (point 2). At remanence, $\langle m_z\rangle$ is close to zero ($\simeq 10^{-3}$). For intermediate negative fields, a deformed vortex state subsists, characterized by $m_z < 0$ everywhere except within the vortex core where the magnetization points up (point 3). The larger negative values of m_z are located at the disk edge. For lower negative field values, the vortex core has switched and the vortex core magnetization points down (point 4). For $H_z < -H_s \simeq -9$ kOe, the disk is uniformly magnetized along the $-z$ axis ($\langle m_z\rangle = -1$). From the half cycle, it appears that a deformed vortex state exists in a large perpendicular field range where $\langle m_z\rangle$ varies linearly with H_z. Interestingly, the perpendicular field evolution of $\langle m_\phi\rangle$ shows that $\langle m_\phi\rangle = 0$ for $|H_z| > H_s$ and $\langle m_\phi\rangle \neq 0$ for $|H_z| < H_s$. $\langle m_\phi\rangle$ passes through a minimum at zero field ($\langle m_\phi\rangle = -1$, case of a clockwise rotational direction). In addition, $\langle m_\phi\rangle$ exhibits a jump at $H_z = H_s$ (first-order phase transition) whereas $\langle m_\phi\rangle$ is continuous at $H_z = -H_s$ (second-order phase transition) for a downward field sweep. This behavior is inverted for an upward field sweep giving rise to a weak hysteresis.

2. Susceptibility spectra

To gain a general view of magnetic excitations occurring in a single ferromagnetic disk, the in-plane susceptibility spectra were computed as functions of frequency and the perpendicular polarizing field H_z (positive values). Figure 4 shows the maps of the imaginary part for the χ_- [Fig. 4(a)] and χ_+ [Fig. 4(b)] spectra for a downward field sweep and a positive field branch. The main features are the following. The χ_- spectrum exhibits multiple resonance lines. In the saturated region ($H_z > H_s \simeq 9$ kOe), several resonance lines are observed with a linear rise of the resonance frequency with H_z. As analyzed in detail in Sec. IV, these lines originate from stationary dipole-exchange SW modes. In the vortex state ($H_z < H_s$), the unique resonance line (case of a thin disk[28]) at low frequency (below 0.5 GHz) is identified as the vortex translation mode. This line is labeled 0_-. Its resonance frequency increases linearly with H_z but its slope is weaker as compared to the ones of the dipole-exchange spin-wave

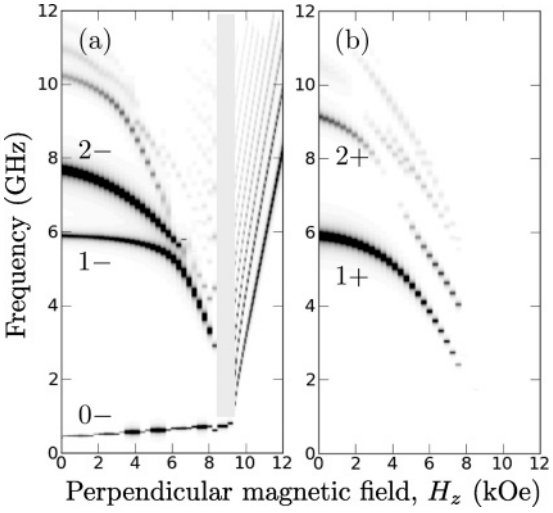

FIG. 4. Computed dynamic susceptibilities in the plane (H_z, f) for a downward field sweep and a positive field branch; (a) χ''_- and (b) χ''_+. The high values are in black and the low ones in light gray. The resonance lines in the vortex state are labeled using a peak numbering. The array with $2R = 1\mu$m is considered. A vertical area near the transition between the saturated and vortex states (a) is masked to avoid confusion due to stroboscopic effect.

modes.[29] At higher frequencies, numerous resonance lines with complex variations of frequency versus H_z are revealed. Their resonance frequencies decrease slowly for increasing H_z at low fields and drop markedly above a critical field that depends on the resonance line. This critical field is lower for high-order resonance lines. Resonance lines labeled 1_- and 2_- display the larger amplitudes. The χ_+ spectrum is simpler. The dipole-exchange SW modes and the vortex translation mode are not excited. Only the high-frequency resonance lines with decreasing resonance frequency for increasing H_z are observed. It should be noted that the positions of the resonance lines for the χ_+ spectrum differ from those of the χ_- spectrum. The two first resonance lines with the higher amplitude are labeled 1_+ and 2_+. From these results, the high-frequency resonance lines with negative frequency slopes at intermediate values of the magnetic field merit a deeper investigation.

IV. COMPARISONS WITH THE EXPERIMENTAL FMR SPECTRA

A. Mode positions

1. Saturated state

The FMR spectra of perpendicularly magnetized isolated disks and disk arrays in the saturated regime have been investigated during the past few years.[38,39] The main result is the emergence of multiple resonance lines identified as standing in-plane spin-wave modes due to the finite disk radius. In this part, the results obtained on our disk array are presented by focusing on the comparisons between the experimental, analytical, and numerical features of FMR spectra. The experimental absorption derivative spectra recorded at $f = 9$ GHz for the continuous Py film and the disk array ($2R = 1\mu$m) are displayed in Fig. 5(a). For the continuous film, the resonance line associated with the uniform precession mode is observed ($H_z = 12.759$ kOe). The patterning of the Py film results in a set of well-defined resonance lines, the fundamental resonance line (highest resonance field value) being shifted toward the low fields by around 1.066 kOe with respect to the uniform mode for the continuous film. The FMR spectrum computed by dynamic micromagnetic simulations using the geometrical and magnetic parameters reported in Sec. II A reproduces very satisfactorily the experimental one [Fig. 5(a)]. The map of the local susceptibility $\chi''_-(r,\phi)$, where r and ϕ are the polar coordinates in the disk plane, computed for the first four SW modes are indicated in Fig. 5(b). These modes possess a radial symmetry and are distinguished by the number of nodes that increases for decreasing resonance fields. These maps confirm the nature of SW modes with in-plane wave vector quantized by the disk edge. The mode index n corresponds to the number of nodes along the dot radius, according to the radial mode profiles $\chi''_-(r)$ displayed at the top of the susceptibility map for each mode. Although the micromagnetic simulations were performed using the free boundary conditions $\frac{\partial \mathbf{m}}{\partial \mathbf{n}} = 0$ at the disk surfaces, the radial profiles reveal values of $\chi''_-(r)$ very close to zero for $r = \pm R$, which reflects a strong pinning at the lateral disk edge. This result is consistent with the theoretical viewpoint. Indeed, it was shown[40] that for a disk with geometrical parameters satisfying $\Lambda < L_z \ll R$ a strong pinning of the dipolar origin

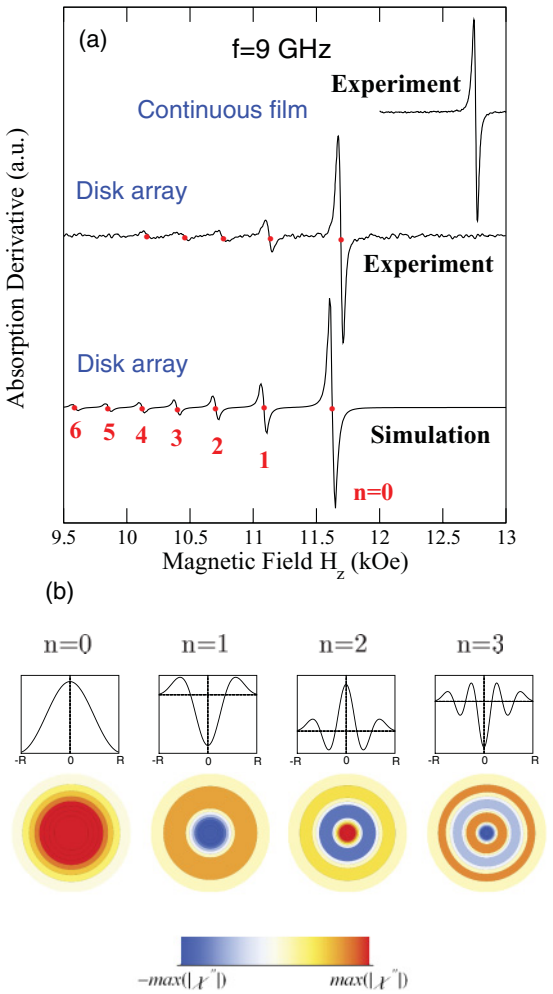

FIG. 5. (Color online) (a) Experimental (Experiment) and numerical (Simulation) field derivatives of the perpendicular power absorption spectra recorded (resp. computed) at $f = 9$ GHz for the disk array with $2R = 1$ μm. The standing in-plane spin-wave resonances are labeled using the radial mode number $n = 0,\ldots,6$. (b) Local susceptibilities for the first four spin-wave modes. For each mode, the mode profile $\chi''_-(r)$ at the positions $\phi = 0$ and $z = 0$ (midplane) and the $\chi''_-(r,\phi)$ map at $z = 0$ are displayed.

is expected for the lowest spin-wave modes. In addition, it should be noted that these modes are found to be invariant along the z axis.

Next, a close examination of the mode positions has been conducted. The comparison between the experimental and computed (numerical and analytical) evolutions of the resonance field as a function of the radial mode index is reported in Fig. 6(a). The analytical evolution of the resonance field is predicted by the dipole-exchange spin-wave model.[38,41] For a perpendicularly magnetized thin disk, the dispersion equation taking into account the quantization of the spin-wave modes and the inhomogeneity of the demagnetizing field inside the element reads[38] $\omega^2(k) = [\omega_H + \omega_M \Lambda^2 k^2][\omega_H + \omega_M(\Lambda^2 k^2 + f(kL))]$, where $\omega_H = \gamma H_i$, $\omega_M = \gamma 4\pi M_S$, $f(kL) = 1 - [1 - \exp(-kL)]/kL$, and k is the modulus of the in-plane wave vector. Assuming a dipolar pinning condition,[40] the allowed wave vectors satisfy the equation $k_n = \beta_n/R$ where

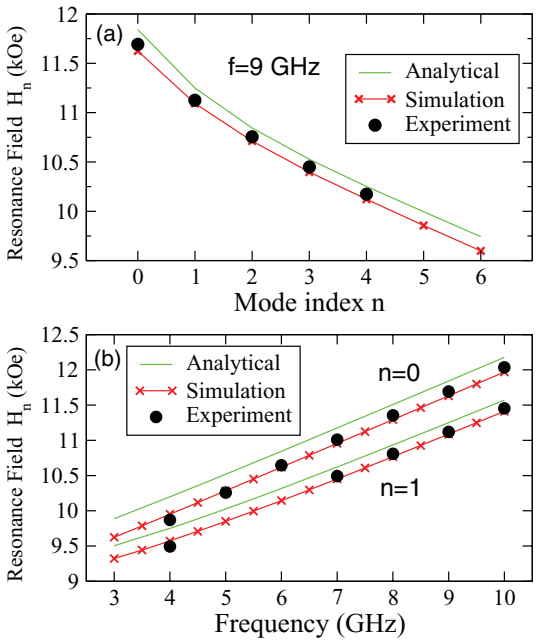

FIG. 6. (Color online) Comparison between the experimental (Experiment, full circles), analytical (Analytical, solid green line), and numerical (Simulation, crosses) evolutions of the resonance fields as function of the mode index at the frequency $f = 9$ GHz (a) and versus frequency for the first two modes $n = 0$ and $n = 1$ (b).

β_n is the $(n+1)$th root of the zeroth-order Bessel function $J_0(\beta_n) = 0$, where $n = 0,1,....$ The effective internal magnetic field H_i is defined by the relation $H_i = H_z - 4\pi M_S N_n(k)$ where $N_n(k) = \frac{2}{R^2 J_1^2(Rk_n)} \int_0^R N(\rho) J_0^2(k_n\rho)\rho\, d\rho$ and $N(\rho)$ is the space-dependent demagnetizing factor for a cylindrical element along the z direction.[42] The results of micromagnetic simulations appear in very good agreement with the experimental ones. The analytical curve shows a similar decrease of the resonance field for increasing the mode number. Nevertheless, the analytical fields are slightly overestimated (by around 2%) with respect to the resonance fields computed by micromagnetic simulations. The experimental, analytical, and numerical frequency dependencies of the resonance fields for the two spin-wave modes ($n = 0$ and $n = 1$) are reported in Fig. 6(b). The experimental and numerical behaviors appear very close to each other, the analytical one being again slightly shifted to higher field values (the maximum deviation reaches 3% at low frequencies). The observed discrepancies between the numerical and analytical behaviors could be partly due to the slight departure from the perfectly uniform static magnetization assumed in the analytical model.

2. *Vortex state at intermediate magnetic fields*

As mentioned in Sec. II B, the four modes experimentally observed at intermediate magnetic fields are characterized by a decrease of their resonance field for increasing frequency. This feature is generally the signature of the reorientation of the magnetization under a noncollinear applied magnetic field. For instance, negative frequency evolutions were reported in soft ferromagnetic stripes in the presence of an in-plane magnetic field applied along the hard axis (transverse applied field).[43,44] Such a behavior has been also revealed in the past for various localized excitations existing in micro/nanostrutures with nonuniform equilibrium magnetization configurations. For soft circular elements in the presence of an in-plane static magnetic field, negative slopes for the curve $\omega(H)$ were evidenced for edge modes[26] and for a mode localized near the shifted vortex core.[27] For Py square elements supporting a Landau state, the in-plane static magnetic applied along the diagonal of the element leads to a shift of the vortex core accompanied with deformations of domains and domain walls. The resonance frequencies of the domains with growing volumes and elongated domain walls decrease for increasing the magnetic field strength.[45] For Py rings with a vortex state, it was shown[46–48] that some azimuthal and radial modes localized in the ring arms present a frequency decrease for increasing the magnetic field if the local static magnetization is antiparallel to the applied magnetic field. On the other hand, negative slopes for the curve $\omega(H)$ can be observed for soft modes in the vicinity of transitions separating two different micromagnetic states.[49,50]

The key point is hence to identify the modes associated with the resonance lines for our perpendicularly magnetized disk at intermediate magnetic fields. Figure 7 displays the comparison between experimental and computed (micromagnetic simulations) spectra at $f = 3.5$ GHz. In this last case, the spectra of the diagonal elements χ''_+, χ''_-, and χ''_{zz} of the susceptibility tensor are superimposed. The micromagnetic simulations enable us to reproduce the four experimentally detected resonance lines. The main resonance line appears in the χ''_- spectrum (line 1_-, resonance field $H_{1_-} = 7.96$ kOe). The χ''_+ spectrum exhibits two weak resonance lines (line 1_+, $H_{1_+} = 7.21$ kOe, and line 2_+, $H_{2_+} = 8.44$ kOe). It should be noted that a small signal exists in the χ''_- spectrum (line 2_-, $H_{2_-} = 8.48$ kOe). The χ''_{zz} spectrum reveals a unique excitation (line 1_z, $H_{1_z} = 7.81$ kOe) whose resonance field is close to the one of the main resonance line 1_-. The appearance of the line 1_z in the experimental spectrum can be explained by the existence of a small RF magnetic field component normal to the sample induced by the finite width of the microstrip line. The map of $\chi''(r,\phi)$ and the mode profiles $\chi''(r)$ are reported in Fig. 7(b) for each mode. A first finding is that the lines 1_+, 1_-, and 2_+ are associated with modes involving the vortex core excitation. The line 1_- results from a mode coupling the vortex core and the disk edge. These two magnetic areas oscillate with opposite phases. In addition, the local susceptibility does not tend toward zero at the disk edge which departs from the strong pinning condition. The lines 1_+ and 2_+ are essentially associated with vortex core modes with different mode profiles. The mode 1_+ spreads out of the vortex core with a radial node close to the disk edge whereas the mode 2_+ is more localized within the vortex core and exhibits two radial nodes. The mode 1_+ does not verify the strong pinning condition at the disk edge in contrast to the mode 2_+. Lastly, the resonance line 1_z is identified as an edge mode without radial node. This mode satisfies the strong pinning condition at the disk edge. It should be remarked that the modes 1_+, 1_z, 1_-, and 2_+ are localized in regions (vortex core and/or disk edge) of strong spatial variations for the static magnetization configuration (see Fig. 3, static magnetization configuration for the point 1).

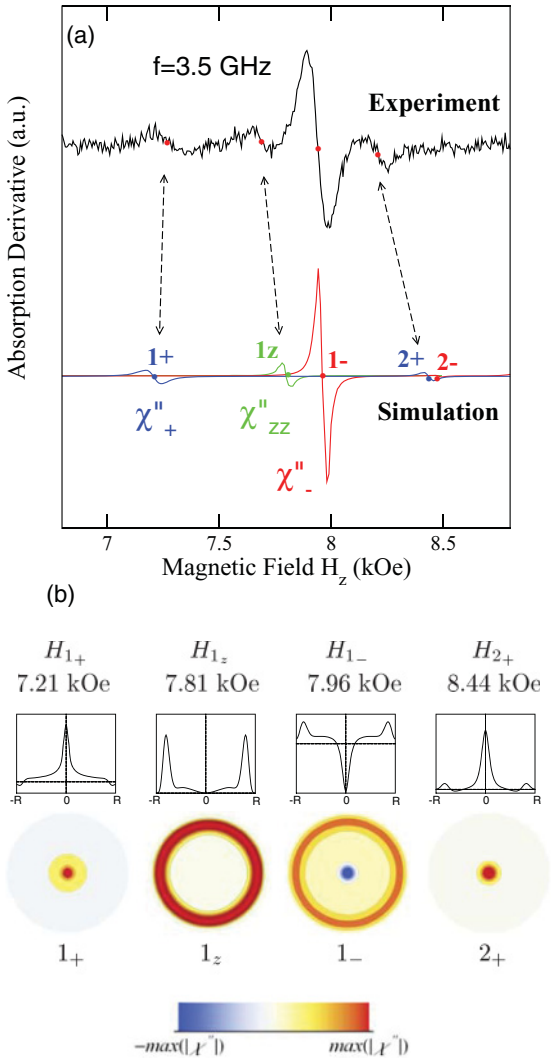

FIG. 7. (Color online) (a) Experimental (Experiment) and numerical (Simulation) field derivatives of the perpendicular power absorption spectra recorded (resp. computed) at $f = 3.5$ GHz for the disk array with $2R = 1$ μm. (b) Local susceptibilities for the first four detected excitations. As in Fig. 5(b), the mode profile $\chi''_-(r)$ at the positions $\phi = 0$ and $z = 0$ and the $\chi''_-(r,\phi)$ map at $z = 0$ are displayed.

The experimental and computed frequency dependencies of the resonance fields for the four resonance lines are reported in Fig. 8. The micromagnetic simulations predict negative slopes for the curves $H_n(f)$, $n = 1_+, 1_z, 1_-, 2_+$, as well. The numerical evolutions are found very close to the experimental ones. A very good agreement is observed between the experimental and computed results for the mode 1_+ and 1_-. A slight discrepancy between the experimental and computed results exists for the modes 1_z and 2_+ (maximum deviation around 6% for the mode1_z at $f = 4.4$ GHz). Two possible causes can be advanced for explaining it. First, an inaccuracy subsists regarding the value of the exchange constant A which is the only parameter not experimentally determined. The adopted value, $A = 1.3 \times 10^{-6}$ erg/cm, lies within the range generally reported for Py film between $A = 1.1 \times 10^{-6}$ erg/cm and $A = 1.4 \times 10^{-6}$ erg/cm. Second,

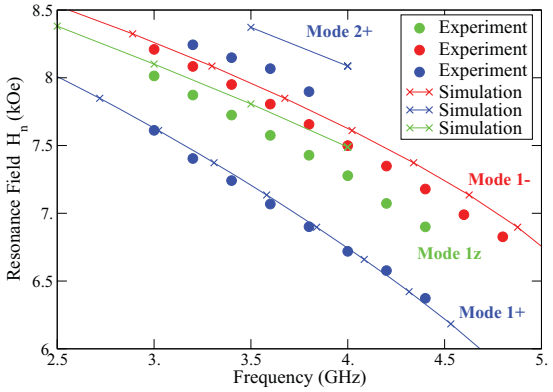

FIG. 8. (Color online) Comparison between the experimental (Experiment, full circles) and numerical (Simulation, crosses) evolutions of the resonance fields as function of frequency for the four resonance lines exhibited in Fig. 7.

the disk thickness is underestimated by around 6% in the micromagnetic simulations.

B. Linewidth

Let us now focus on the analysis of resonance linewidths both in saturated and vortex states. Figure 9 shows the experimental and computed frequency dependencies of ΔH_{pp} for the dipole exchange mode $n = 0$ and for the main resonance line 1_- in the vortex state at intermediate magnetic fields. For the mode $n = 0$, the micromagnetic simulations predict a linear variation for $\Delta H_{pp}(f)$. The experimental values appear to be very close to the computed ones. A linear variation is experimentally obtained for a frequency greater than 6 GHz resulting in the following values: $\alpha = 6.9 \pm 0.1 \times 10^{-3}$ and $\Delta H_{pp,0} = 16.2 \pm 1.2$ Oe. Two comments can be added. First, the extrinsic contribution $\Delta H_{pp,0}$ is not taken into account in the micromagnetic simulations. Second, the value of $\Delta H_{pp,0}$ for the array is in excess with respect to the one for the continuous film ($\Delta H_{pp,0} = 2.4 \pm 0.9$ Oe). Imperfections

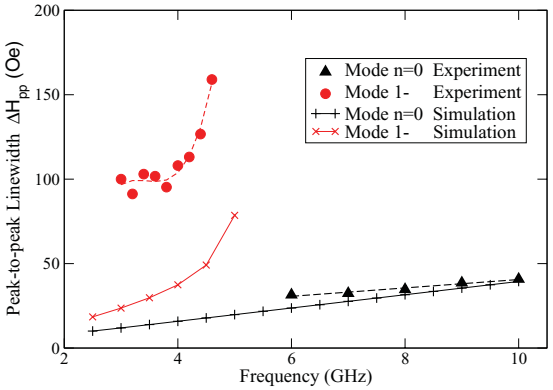

FIG. 9. (Color online) Comparison between the experimental (Experiment, full symbols) and numerical (Simulations, crosses and plus) evolutions of the resonance linewidths as function of frequency for the dipole-exchange mode $n = 0$ (saturated state) and for mode 1_- (vortex state). The disk array with $2R = 1$ μm is considered. The dashed lines are fits of experimental data. The solid lines are guides for the eye.

caused by the patterning process (edge and surfaces roughness, shape and size fluctuations) are responsible for this variation. For the mode 1_-, the curve $\Delta H_{pp}(f)$ looks quite different. The main features can be synthesized as follows. (i) The values of ΔH_{pp} for mode 1_- are always greater than the ones reported for mode $n = 0$. From micromagnetic simulations, the ratio $\Delta H_{pp,\mathrm{vor}}/\Delta H_{pp,\mathrm{sat}}$ varies between 2 ($f = 3$ GHz) and 4 ($f = 5$ GHz). (ii) Mode 1_- broadens rapidly for $f > 4$ GHz with an asymptotic behavior around $f = 5.5$ GHz. (iii) The experimental and numerical ΔH_{pp} curves display the same profiles but the experimental values exceed the numerical ones (up to a factor 3 for $f = 4.6$ GHz). It should be noted that the spectral range where the resonance line 1_- broadens drastically corresponds to the nearly flat part of the dispersion curve $f(H_z)$ at low and intermediate magnetic fields [see Fig. 4(a)].

Analysis of the resonance linewidths in the vortex states have been relatively rarely reported.[51] For the vortex translation mode, it has been established that the resonance linewidth depends on the geometrical parameters of the magnetic structures.[52] For a disk element, the zero-field vortex resonance can be described using an effective damping parameter related to the Gilbert parameter by the relation $d = \alpha[1 + \ln(R/R_c)/2]$ where R_c is the thickness-dependent vortex core radius.[52] This expression has been successfully tested using experimental vortex resonance data.[51,52] For the range of aspect ratio currently encountered, d is typically three times as large as α. A similar widening of the resonance lines associated with modes located in the vicinity of the shifted vortex core for a disk element in the presence of an applied DC magnetic field was reported as well.[27]

V. MRFM EXPERIMENTS ON AN INDIVIDUAL NiMnSb DISK

To confirm these findings, we have also studied the magnetization dynamics in an individual ferromagnetic disk, using a room temperature magnetic resonance force microscope (MRFM).[39] In these experiments, the sample is an isolated disk of diameter $2R = 1$ μm and thickness $L_z = 44$ nm, patterned from a NiMnSb film grown by molecular beam epitaxy on InP(001).[53] The bias magnetic field H_z is applied perpendicularly to the disk plane, and a broadband microwave antenna evaporated on top of the NiMnSb disk supplies an in-plane microwave magnetic field δh_{rf} (linearly polarized). A spherical magnetic probe attached at the end of a very soft cantilever is dipolarly coupled to the sample and is positioned 1.5 μm above its center. It makes it possible to monitor the variation of the averaged component M_z in the NiMnSb disk due to the SW modes excited by the microwave field. This mechanical detection of magnetic resonance is very sensitive, and can be used to probe vortex core dynamics in individual submicrometer-sized disks.[29,51,54]

MRFM spectra can be obtained at fixed excitation frequency f by sweeping the perpendicular bias field H_z and recording the cantilever motion. Several of them are plotted in Fig. 10(a), where f is ranging between 1.8 and 3.1 GHz and $\delta h_{rf} \simeq 0.3$ Oe. The detailed magnetic characterization of the NiMnSb disk performed in Ref. 29 previously yielded its saturation field, $H_s = 8.1$ kOe. When $H_z > H_s$, the sample is fully saturated along its normal, and a series of stationary

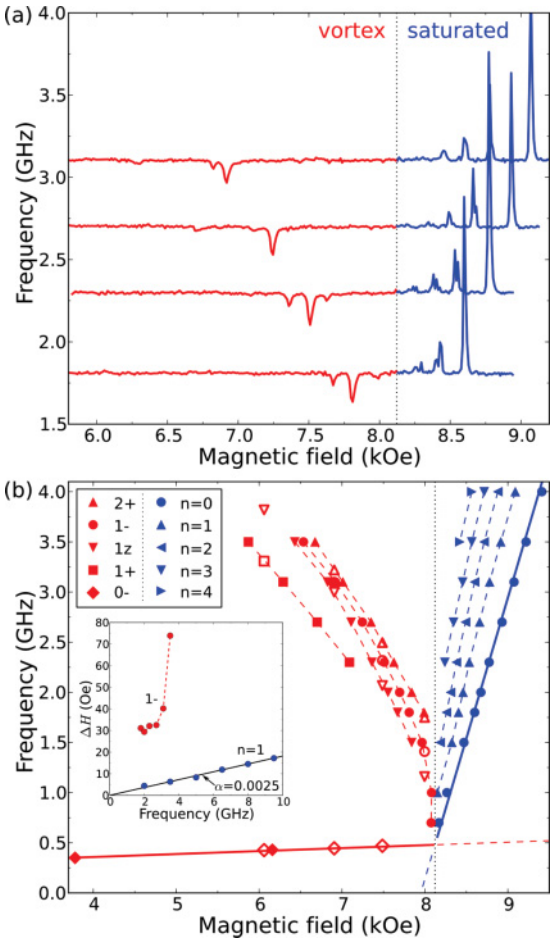

FIG. 10. (Color online) (a) Resonance spectra obtained by magnetic resonance force microscopy (MRFM) on an individual disk of NiMnSb ($L_z = 44$ nm, $2R = 1$ μm). The dotted vertical line displays the saturation field $H_s = 8.1$ kOe of the NiMnSb disk, separating the vortex state from the saturated state. (b) Dispersion relation of the different spin-wave modes observed experimentally. Solid symbols have been obtained from field-sweep MRFM spectra at fixed frequency [see panel (a)]. Open symbols have been obtained from frequency-sweep MRFM spectra at fixed magnetic field. Solid lines in the saturated ($H_z > H_s$) and vortex states ($H_z < H_s$) are theoretical predictions from Eqs. (1) and (2) of Ref. 29, respectively. Dashed lines are guides to the eye. The inset shows the variation of the full linewidth ΔH as a function of frequency for the modes $n = 0$ and 1_-.

SW modes[38] can be observed in the spectra of Fig. 10(a) (see blue region). The positive MRFM peaks correspond here to the decrease of the longitudinal component M_z due to the precession of the magnetization around its equilibrium axis z when SW modes are excited in the disk.[39] We note in passing, that the low Gilbert constant $\alpha = 0.0025$ deduced from measurements of the linewidth of the fundamental mode $n = 0$ is typical from the half-Heusler NiMnSb alloy.[55] When $H_z < H_s$, the NiMnSb disk is in the vortex state,[29] and up to four well-resolved SW modes can still be observed at lower field, in the red region of the spectra displayed in Fig. 10(a). The similarity of these modes to those observed in the broadband FMR experiment of Fig. 7(a), performed

on an array of Py disks, is striking. The relative amplitudes and positions are very consistent, the smaller resonance fields observed for the NiMnSb disk being mainly ascribed to its smaller magnetization compared to Py.[29]

To gain further insight about the nature of the SW modes which can be excited above and below the saturation field, we have plotted in Fig. 10(b) their frequency-field dispersion relation in blue and red symbols, respectively. We have labeled the different SW modes according to the mode identification made in Sec. IV [see Figs. 5(a) and 7(a)] on the Py disk array. In the saturated state, the lowest energy SW mode is the most uniform mode $n = 0$, and its dispersion relation follows a standard Kittel equation [blue continuous line in Fig. 10(b); see Eq. (1) of Ref. 29]. The higher energy modes correspond to harmonics with an increasing number of precession nodes in the radial direction [see Fig. 5(b), mode profiles from simulations in the saturated state]. In the vortex state, the fundamental SW mode is the gyrotropic mode (labeled 0_-), whose frequency increases linearly with the perpendicular bias field [red continuous line in Fig. 1(b), see Eq. (2) of Ref. 29]. The higher energy modes correspond either to vortex core excitations or coupled modes between the vortex core and the disk edge, as determined above from micromagnetic simulations [see Fig. 7(b), mode profiles from simulations in the vortex state]. As observed in the Py disks, the frequency of these modes in the NiMnSb disk decreases with the perpendicular magnetic field, and goes to zero at the compensation point $H_z = H_s$, where they become soft.[43] This negative slope of the frequency-field dispersion relation is related to the decrease of the effective field probed by these SW modes in the unsaturated state as H_z increases. It should be noted that the MRFM signal corresponding to these modes in the vortex state is negative, see Fig. 10(a), meaning that the averaged component of magnetization M_z along the applied field H_z increases at resonance, in contrast to the standard case observed in the saturated state. Finally, the experimental frequency dependencies of the full linewidth ΔH for the mode $n = 0$ and 1_- are reported in the inset of Fig. 10(b). These variations are quite similar to those observed for the Py disk array (see Fig. 9), namely, a linear evolution for the mode $n = 0$ and a rapid increase for the mode 1_-.

VI. CONCLUSION

An in-depth analysis of the linear excitation spectrum in perpendicularly magnetized disks was performed both in the saturated and vortex states using ferromagnetic resonance spectroscopy and micromagnetic simulations. The experimental microwave absorption spectra exhibit a set of discrete signals ascribed to dipole-exchange SW modes quantized by the disk edge in the saturated state whereas multiple resonance lines with negative slopes for the dispersion relation $\omega(H_z)$ are revealed in the vortex state at intermediate magnetic fields. These results have been obtained both for a Py disk array probed by a broadband FMR spectrometer with a microstrip line and on a single NiMnSb disk by means of MRFM measurements. The remarkable similarity between these results demonstrates the consistency of experimental data and highlights the robustness of the physical phenomenon. The micromagnetic simulations conducted on a Py disk array (regime of negligible coupling between the disks) allow us to identify all the excitations experimentally detected. In particular, the four excitations occurring in the deformed vortex state arise from vortex core, disk edge, and coupled vortex core/disk edge modes. In addition, the micromagnetic simulations reproduce very satisfactorily the experimental $\omega(H_z)$ curves. The linewidth of the more intense coupled vortex core/disk edge mode is larger than the ones of dipole-exchange SW modes and grows markedly with frequency in agreement with the predicted evolution coming from micromagnetic simulations. This striking behavior seems to be related to the flattening of the frequency-field dispersion curve at low and intermediate magnetic fields.

These results contribute to a better understanding of the magnetic excitations existing under a perpendicular magnetic field in vortex-state elements. One important finding is that various modes including vortex core oscillations were evidenced. The effects of the disk size and the magnetostatic coupling between the disks within arrays on the dispersion relations of these excitations merit further investigation. Regarding this last point, it should be underlined that the comparisons between MRFM measurements in a single disk and FMR ones in disk arrays are very fruitful. These combined experimental approaches could be applied to various nanostructures with nonuniform magnetization configurations.

ACKNOWLEDGMENTS

B.P., G.d.L., and O.K. are grateful to L. W. Molenkamp for providing the NiMnSb sample. The research work involving MRFM was partially supported by the French Grant Voice ANR-09-NANO-006-01.

*nicolas.vukadinovic@dassault-aviation.com

[1] R. P. Cowburn, D. K. Koltsov, A. O. Adeyeye, M. E. Welland, and D. M. Tricker, Phys. Rev. Lett. **83**, 1042 (1999).
[2] K. Y. Guslienko, B. A. Ivanov, V. Novosad, Y. Otani, H. Shima, and K. Fukamichi, J. Appl. Phys. **91**, 8037 (2002).
[3] B. A. Ivanov and C. E. Zaspel, Appl. Phys. Lett. **81**, 1261 (2002).
[4] J. P. Park, P. Eames, D. M. Engebretson, J. Berezovsky, and P. A. Crowell, Phys. Rev. B **67**, 020403 (2003).
[5] V. Novosad, F. Y. Fradin, P. E. Roy, K. S. Buchanan, K. Y. Guslienko, and S. D. Bader, Phys. Rev. B **72**, 024455 (2005).
[6] K. Y. Guslienko, X. F. Han, D. J. Keavney, R. Divan, and S. D. Bader, Phys. Rev. Lett. **96**, 067205 (2006).
[7] R. Zivieri and F. Nizzoli, Phys. Rev. B **71**, 014411 (2005).
[8] K. Y. Guslienko, W. Scholz, R. W. Chantrell, and V. Novosad, Phys. Rev. B **71**, 144407 (2005).
[9] C. E. Zaspel, E. S. Wright, A. Y. Galkin, and B. A. Ivanov, Phys. Rev. B **80**, 094415 (2009).

[10]V. Novosad, M. Grimsditch, K. Y. Guslienko, P. Vavassori, Y. Otani, and S. D. Bader, Phys. Rev. B **66**, 052407 (2002).
[11]M. Buess, R. Höllinger, T. Haug, K. Perzlmaier, U. Krey, D. Pescia, M. R. Scheinfein, D. Weiss, and C. H. Back, Phys. Rev. Lett. **93**, 077207 (2004).
[12]L. Giovannini, F. Montoncello, F. Nizzoli, G. Gubbiotti, G. Carlotti, T. Okuno, T. Shinjo, and M. Grimsditch, Phys. Rev. B **70**, 172404 (2004).
[13]I. Neudecker, K. Perzlmaier, F. Hoffmann, G. Woltersdorf, M. Buess, D. Weiss, and C. H. Back, Phys. Rev. B **73**, 134426 (2006).
[14]K. Vogt, O. Sukhostavets, H. Schultheiss, B. Obry, P. Pirro, A. A. Serga, T. Sebastian, J. Gonzalez, K. Y. Guslienko, and B. Hillebrands, Phys. Rev. B **84**, 174401 (2011).
[15]V. V. Naletov, G. de Loubens, G. Albuquerque, S. Borlenghi, V. Cros, G. Faini, J. Grollier, H. Hurdequint, N. Locatelli, B. Pigeau, A. N. Slavin, V. S. Tiberkevich, C. Ulysse, T. Valet, and O. Klein, Phys. Rev. B **84**, 224423 (2011).
[16]J. P. Park and P. A. Crowell, Phys. Rev. Lett. **95**, 167201 (2005).
[17]F. Hoffmann, G. Woltersdorf, K. Perzlmaier, A. N. Slavin, V. S. Tiberkevich, A. Bischof, D. Weiss, and C. H. Back, Phys. Rev. B **76**, 014416 (2007).
[18]K. Y. Guslienko, A. N. Slavin, V. Tiberkevich, and S. K. Kim, Phys. Rev. Lett. **101**, 247203 (2008).
[19]A. A. Awad, K. Y. Guslienko, J. F. Sierra, G. N. Kakazei, V. Metlushko, and F. G. Aliev, Appl. Phys. Lett. **96**, 012503 (2010).
[20]J. Shibata, K. Shigeto, and Y. Otani, Phys. Rev. B **67**, 224404 (2003).
[21]J. Shibata and Y. Otani, Phys. Rev. B **70**, 012404 (2004).
[22]K. Y. Guslienko, K. S. Buchanan, S. D. Bader, and V. Novosad, Appl. Phys. Lett. **86**, 223112 (2005).
[23]A. Y. Galkin, B. A. Ivanov, and C. E. Zaspel, Phys. Rev. B **74**, 144419 (2006).
[24]A. Vogel, A. Drews, T. Kamionka, M. Bolte, and G. Meier, Phys. Rev. Lett. **105**, 037201 (2010).
[25]F. Boust and N. Vukadinovic, IEEE Trans. Magn. **47**, 349 (2011).
[26]K. Rivkin, W. Xu, L. E. D. Long, V. V. Metlushko, B. Ilic, and J. B. Ketterson, J. Magn. Magn. Mater. **309**, 317 (2007).
[27]F. G. Aliev, J. F. Sierra, A. A. Awad, G. N. Kakazei, D. S. Han, S. K. Kim, V. Metlushko, B. Ilic, and K. Y. Guslienko, Phys. Rev. B **79**, 174433 (2009).
[28]F. Boust and N. Vukadinovic, Phys. Rev. B **70**, 172408 (2004).
[29]G. de Loubens, A. Riegler, B. Pigeau, F. Lochner, F. Boust, K. Y. Guslienko, H. Hurdequint, L. W. Molenkamp, G. Schmidt, A. N. Slavin, V. S. Tiberkevich, N. Vukadinovic, and O. Klein, Phys. Rev. Lett. **102**, 177602 (2009).
[30]V. Novosad, K. Y. Guslienko, H. Shima, Y. Otani, S. G. Kim, K. Fukamichi, N. Kikuchi, O. Kitakami, and Y. Shimada, Phys. Rev. B **65**, 060402(R) (2002).
[31]D. Pain, M. Ledieu, O. Acher, A. L. Adenot, and F. Duverger, J. Appl. Phys. **85**, 5151 (1999).
[32]J. Ben Youssef, N. Vukadinovic, D. Billet, and M. Labrune, Phys. Rev. B **69**, 174402 (2004).
[33]S. Labbé and P. Y. Bertin, J. Magn. Magn. Mater. **93**, 206 (1999).
[34]N. Vukadinovic and F. Boust, Phys. Rev. B **75**, 014420 (2007).
[35]M. Sparks, *Ferromagnetic Relaxation Theory* (McGraw-Hill, New York, 1964).
[36]N. Vukadinovic, M. Labrune, J. Ben Youssef, A. Marty, J. C. Toussaint, and H. Le Gall, Phys. Rev. B **65**, 054403 (2001).
[37]This mesh size is too coarse for capturing accurately the zero-field resonance frequency of the vortex translation mode where the vortex core has its minimum value.
[38]G. N. Kakazei, P. E. Wigen, K. Y. Guslienko, V. Novosad, A. N. Slavin, V. O. Golub, N. A. Lesnik, and Y. Otani, Appl. Phys. Lett. **85**, 443 (2004).
[39]O. Klein, G. de Loubens, V. V. Naletov, F. Boust, T. Guillet, H. Hurdequint, A. Leksikov, A. N. Slavin, V. S. Tiberkevich, and N. Vukadinovic, Phys. Rev. B **78**, 144410 (2008).
[40]K. Y. Guslienko and A. N. Slavin, Phys. Rev. B **72**, 014463 (2005).
[41]B. A. Kalinikos and A. N. Slavin, J. Phys. C **19**, 7013 (1986).
[42]S. Tandon, M. Beleggia, Y. Zhu, and M. D. Graef, J. Magn. Magn. Mater. **271**, 9 (2004).
[43]M. Bailleul, D. Olligs, and C. Fermon, Phys. Rev. Lett. **91**, 137204 (2003).
[44]C. Bayer, J. P. Park, H. Wang, M. Yan, C. E. Campbell, and P. A. Crowell, Phys. Rev. B **69**, 134401 (2004).
[45]M. Bailleul, R. Höllinger, K. Perzlmaier, and C. Fermon, Phys. Rev. B **76**, 224401 (2007).
[46]G. Gubbiotti, M. Madami, S. Tacchi, G. Carlotti, H. Tanigawa, T. Ono, L. Giovannini, F. Montoncello, and F. Nizzoli, Phys. Rev. Lett. **97**, 247203 (2006).
[47]I. Neudecker, M. Klaui, K. Perzlmaier, D. Backes, L. J. Heyderman, C. A. F. Vaz, J. A. C. Bland, U. Rüdiger, and C. H. Back, Phys. Rev. Lett. **96**, 057207 (2006).
[48]F. Giesen, J. Podbielski, B. Botters, and D. Grundler, Phys. Rev. B **75**, 184428 (2007).
[49]F. Montoncello, L. Giovannini, F. Nizzoli, P. Vavassori, and M. Grimsditch, Phys. Rev. B **77**, 214402 (2008).
[50]N. Vukadinovic and F. Boust, Phys. Rev. B **84**, 224425 (2011).
[51]B. Pigeau, G. de Loubens, O. Klein, A. Riegler, F. Lochner, G. Schmidt, and L. W. Molenkamp, Nature Phys. **7**, 26 (2011).
[52]K. Y. Guslienko, Appl. Phys. Lett. **89**, 022510 (2006).
[53]P. Bach, S. D. Bader, C. R. Rüster, C. Gould, C. R. Becker, G. Schmidt, L. W. Molenkamp, W. Weigand, C. Kumpf, E. Umbach, R. Urban, and G. W. B. Heinrich, Appl. Phys. Lett. **83**, 521 (2003).
[54]B. Pigeau, G. de Loubens, O. Klein, A. Riegler, F. Lochner, G. Schmidt, L. W. Molenkamp, V. S. Tiberkevitch, and A. N. Slavin, Appl. Phys. Lett. **96**, 132506 (2010).
[55]B. Heinrich, G. Woltersdorf, R. Urban, O. Mosendz, G. Schmidt, P. Bach, L. W. Molenkamp, and E. Rozenberg, J. Appl. Phys. **95**, 7462 (2004).